Transition State Spectroscopy of the Photoinduced Ca + CH_3F Reaction. 2. Experimental and Ab Initio Studies of the Free Ca···FCH_3 Complex

J.-M. Mestdagh,*,† F. Spiegelman,‡ E. Gloaguen,† M. Collier,† F. Lepetit,† M.-A. Gaveau,† C. Sanz Sanz,§ and B. Soep†

Laboratoire Francis Perrin (CNRS-URA-2453), DSM/DRECAM/Service des Photons, Atomes et Molécules, CEA Saclay, F-91191 Gif-sur-Yvette Cedex, France, Laboratoire de Physique Quantique (UMR 5626 du CNRS), IRSAMC, Université Paul Sabatier, 118 Route de Narbonne, F31062 Toulouse Cedex, France, Unidad Asociada UAM-CSIC, Departamento de Química Física, Facultad de Ciencias C-XIV, Universidad Autónoma de Madrid, 28049 Madrid, Spain, and Instituto de Matemáticas y Física Fundamental, CSIC, Serrano 123, 28006 Madrid, Spain

Received: December 23, 2005; In Final Form: April 14, 2006

The Ca* + CH_3F → CaF* + CH_3 reaction was photoinduced in 1:1 Ca···CH_3F complexes formed in a supersonic expansion. The transition state of the reaction was explored by monitoring the electronically excited product, CaF, while scanning the laser that turns on the reaction. Moreover, the electronic structure of the Ca···FCH_3 system was studied using ab initio methods by associating a pseudopotential description of the [Ca^{2+}] and [F^{7+}] cores, a core polarization operator on calcium, an extensive Gaussian basis and a treatment of the electronic problem at the CCSD(T) (ground state) and RSPT2 (excited states) level. In this contribution we present experimental results for the free complex and a comparison with the results of a previous experiment where the Ca···CH_3F complexes are deposited at the surface of large argon clusters. The ab initio calculations allowed an interpretation of the experimental data in terms of two reaction mechanisms, one involving a partial charge transfer state, the other involving the excitation of the C−F stretch in the CH_3F moiety prior to charge transfer.

1. Introduction

The present paper is the second of a series[1] concerning the reaction

$$Ca + CH_3F \rightarrow CaF + CH_3 \qquad \Delta H = -80\ \text{kJ/mol} = -0.83\ \text{eV} \quad (1)$$

The energetics are taken from refs 2 and 3. Because the bonding in CaF is ionic, the mechanism of the reaction could be considered as a simple harpoon reaction where a low ionization energy atom, Ca, transfers one of its valence electrons to an electron accepting molecule, CH_3F. However, a complication arises due to the internal degrees of freedom of CH_3F that has motivated our interest to this system. Methyl fluoride is representative of molecules that require deformation to become an electron attractor. No bound state of an additional electron exists at the equilibrium geometry of this molecule and the C−F bond has to be stretched, for the molecule to attach an extra electron[4] and become reactive. Hence, the dynamics of the reaction are expected to be more complex than suggested by the simple harpoon model. In particular, the transition state for a reaction to occur in excited electronic states may involve a geometrically wider range of the potential energy surfaces (PES's) than the pointlike crossing picture usually invoked in the standard harpooning mechanism. Moreover, as in the related Li + CH_3F reaction,[5] a barrier is expected to block the ground state reaction 1, although it is exothermic. Evidence of this property has already been shown experimentally in the ground state because a 1:1 nonreactive Ca···CH_3F complex could be stabilized on a large argon cluster (see paper 1 of this series[1]).

This class of electron transfer reactions where the molecular reactant needs deformation to attach an extra electron is generally encountered in reactions of alkali and alkaline earth atoms with methyl halide and hydrogen halide molecules. Some of the available literature, both experimental and theoretical is reviewed below. It mostly concerns alkali-hydrogen halides systems.

Experimentally, the dynamics of these reactions has been explored both in bimolecular collisions[6−8] and in van der Waals complexes by analyzing action spectra when turning on the reaction with lasers and monitoring one of the reaction products. The Na/HF,[9] Li, Na/HF, CH_3F,[5,10,11] Na_2/CH_3Cl,[12] Ca/HX[13−16] and Ba/CH_3F[17−22] systems were explored using the latter technique. Real-time studies have also been performed on the Ba/CH_3F system.[23−27] For all the studies appearing in the literature the observed branching to reaction is quite complex. For example, the Na/HF study reveals that exciting the H−F stretch promotes the electron transfer step prior to reaction[9] and the Ba/CH_3F studies indicate that the reaction proceeds only after the initial electronic excitation has been transferred to a lower electronic state.

Potential and dynamical calculations are also available, essentially for alkali/hydrogen halide systems.[9,28−36] In particular, the Na/HF system has benefited from extensive ab initio energetics and transition dipole moment calculations that yielded an action spectrum in good agreement with the experimental data.[35,36] Concerning systems that contain an alkaline earth atom, besides the pioneering work of Isaacson and Muckerman on

† CEA Saclay.
‡ Université Paul Sabatier.
§ Universidad Autónoma de Madrid and CSIC.

10.1021/jp057483j CCC: $33.50
Published on Web 05/19/2006

Ca+HCl,[37] an extensive exploration of the ground state PES is available for Be/HF[38] as well as information on excited PES and the corresponding excited state dynamics for Ca/HCl[39−42] and Ca, Ba/CH_3F.[24,40] The work on Ca/CH_3F[40] is a semiclassical treatment of the dynamics, based on multipolar expansion of the electrostatic interaction between Ca and CH_3F. It is aimed at unraveling steric effects in the bimolecular collision between Ca(4s3d ^{1}D) and CH_3F, spatially oriented.

Process 1 is particularly attractive, given the results published in the first paper of this series, a cluster isolated chemical reaction (CICR) study where the van der Waals complex Ca···CH_3F is deposited at the surface of a large argon cluster.[1] When the laser is scanned to turn the reaction on, a broad structured action spectrum was found. It appears quite blue-shifted, from the 4s4p ^{1}P ← 4s^2 ^{1}S calcium resonance transition at 422.8 nm, extending from 360 and 420 nm where no transition of calcium is expected. In that work it was concluded that a local excitation of the sole calcium atom could not account for such a band. Two explanations were proposed, based either on purely electronic or on purely dynamical arguments. The first one implies a significant alteration of the calcium electronic structure that brings a level of calcium within the excitation region. This can be due either to a substantial electron transfer between Ca and CH_3F in the excited state or to the promotion of the excited electron to a Rydberg orbital, stabilized by the interaction with CH_3F. The second tentative explanation was invoked due to the observation of structures in the action spectrum, an observation that makes the present Ca/CH_3F system very different from the apparently similar Ba/CH_3F system (Ca and Ba are both alkaline earth atoms) studied in the groups of Ureña[17−22] and Radloff.[23−27] The structures observed in the Ca/CH_3F system were tentatively assigned to the C−F stretch in the CH_3F molecule, suggesting that this stretch plays an important role in the dynamics of turning on the reaction. Depositing one (or more) quantum on this vibration would lead to a substantial blue shift of the action spectrum with respect to the calcium resonance line, in agreement with the experiment.

The present work aims at clarifying the issues mentioned above on the nature of the electronic transitions that promote the reaction and on the influence of the dynamics in the observed action spectrum. In particular, we would like to know whether the laser excitation directly turns on a charge transfer reaction mechanism. For this purpose, an experimental investigation was achieved, where the Ca···CH_3F complex is "*free*" instead of being deposited on an argon cluster as in CICR experiments. Our expectation is that the solvation of a charge transfer intermediate by the argon environment of CICR experiments may red shift the corresponding part of the action spectrum. Comparing action spectra from CICR and free cluster experiments would then help to disentangle charge transfer from other reaction paths.

In parallel with the experimental investigation, we have carried out detailed ab initio calculations of the PES's of Ca + CH_3F in the entrance channel, considering all the excited states of calcium up to Ca*(4s5s ^{1}S). The electronic problem was treated within a CASPT2 type scheme within a pseudopotential description of Ca and F. Moreover, because, as mentioned, charge transfer is expected to play a crucial role, we have also determined the dipole moments of various states along the entrance channel of the reaction.

2. Experiment

A full report of the experimental technique will appear in paper 3 of this series. Briefly, a He/CH_3F/Ca mixture is expanded into a vacuum to generate a supersonic beam containing the Ca···CH_3F complex. Laser evaporation is used to produce Ca in the gas phase. In addition to the desired complex, the beam contains other compounds: free Ca, CH_3F and CaF that were generated by the laser ablation of the Ca rod in the He/CH_3F mixture. The beam also carries clusters of these compounds.

The Ca···CH_3F complex is excited selectively by a pulsed laser (the pump) with a nanosecond pulse width, tuned to absorption bands of the complex. Depending on the wavelength domain, the same laser or a second one (the probe) ionizes the desired compounds resulting from the laser driven reaction (and undesired compounds also present in the beam). The photoions are detected using time-of-flight mass spectrometry. In the present work, the CaF^+ ion signal is monitored as a function of the pump wavelength. As always, in laser ablation experiments, the choice of expansion conditions, pulse energy and focusing of the ablation laser is quite difficult to get a signal originating reliably from reactions within the desired complex. The fluence of the pump laser (and probe laser when two lasers are used) is also of importance in this respect.

The pump laser is tuned over two spectral ranges, 535−421 nm and 415−353 nm, on each side of the Ca(4s4p ^{1}P ← 4s^2 ^{1}S) resonant transition at 422.8 nm. The latter spectral range includes the band already reported in our previous CICR experiment.[1]

In the red range, the photon energy is not sufficient to allow for both the excitation of the complex and the ionization of the reaction compounds. Ionization is thus performed using a second laser, the probe laser, operating at 354.7 nm and delayed by 5 ns with respect to the pump laser to ascertain that the probe operates on an excited neutral. Energetically, the probe pulses allow us to ionize CaF when excited in the $B^2\Sigma^+$ state. Recording the corresponding signal while scanning the pump laser provides the so-called action spectra of the reaction forming CaF($\geq B^2\Sigma^+$). As it will appear in paper 3 of this series, in contrast to signals measured in the blue range (see below), signals measured in the present red range could not be normalized to the concentration of the Ca···CH_3F complex. For this reason, only the overall location and extension of the band observed in this spectral region will be considered below, not its shape and detailed structure.

In the blue range, the photon energy is sufficient to, at once, turn on the reaction in the complex with one photon and further ionize the electronically excited products of the reaction with one or two additional photons. Given the ionization energy of CaF, the ionization can proceed either from a resonant two photon process on CaF($A^2\Pi$ or $B^2\Sigma^+$) with a low vibrational energy or from a single photon process on the same electronic states of CaF but with a substantial vibrational excitation. In both cases, the CaF^+ signal observed while scanning the laser documents the action spectrum, i.e., the reactive yield of CaF(A,B) from the excited complex. The ion signals measured here could be normalized to the concentration of the complex because a signal proportional to this concentration was available. Hence, a detailed analysis of structures in the measured spectrum is meaningful. Nevertheless, the shape of the spectrum is not corrected for variations of the ionization efficiency as a function of the CaF internal energy. Potentially, this affects the relative intensities of the structures that appear in the spectrum because the internal excitation of CaF may vary from one end of the spectrum to the other. However, this does not affect the localization of the structures, the only question to be addressed

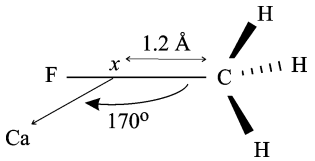

Figure 1. Geometry of the Ca···CH_3F complex used for the potential energy calculations reported in Figures 5 and 6.

in the present paper (a fully corrected spectrum will appear and will be discussed in paper 3 of this series).

3. Calculations

The calculations have been conducted using the MOLPRO ab initio package.[43] They aim to describe the ground and electronic states of the Ca/CH_3F system as Ca approaches CH_3F. A limited exploration of the corresponding PES's along the C−F coordinate is also performed as well as a rough exploration of the topology of the ground state surface.

3.1. Geometrical Considerations. In the context of the bimolecular reaction 1, the approach between Ca and CH_3F corresponds to the entrance channel of the reaction. We anticipate earlier in the Introduction that, although the ground state reaction forming CaF + CH_3 is exothermic, it is blocked by a barrier. The experimental part of the present work took advantage of this property and indirectly confirmed the existence of such a barrier because it was possible to form a nonreactive Ca···CH_3F complex from which the reaction is turned on by photoexcitation. This was observed also in paper 1 of this series.[1] Hence, a local van der Waals well is expected to exist in the entrance channel of the ground state reaction that defines the equilibrium geometry of the complex. Its location was investigated in the present work, using a geometry optimization at the CCSD(T) level, corrected for the basis set superposition error (BSSE) with respect to the dissociation channel Ca + CH_3F.

The approach between Ca and CH_3F is described in Figure 1 by the distance between Ca and a dummy point *x*. Point *x* is located along the C−F bond at 1.2 Å from C. For the potential curve calculations, Ca approaches *x* along a line defined by the C−*x*−Ca angle set to 170°. The values 1.2 Å and 170° are somewhat arbitrary. They were chosen because the corresponding "Ca trajectory" is believed to be representative of an approach toward the F end of the CH_3F molecule.

3.2. Electronic Problem. As already mentioned, the present calculations aim at predicting the excited PES's of Ca···CH_3F. This implies in particular that the asymptotic energies at large separations between Ca and CH_3F are well predicted; i.e., a correct description of the transition energies of calcium is needed here up to 33 000 cm^{-1}. For this purpose, we used the technique successfully applied in ref 44 where the core electrons of calcium are described by a [Ca^{2+}] effective potential, complemented by a core-polarization operator to account for the significant electric dipole polarizability of [Ca^{2+}] ($\alpha = 3.171$ a_0^3). The cutoff function used here to calculate the corresponding correction is that of ref 45, with the cutoff parameter set to 0.365 au. An extensive uncontracted 12s,8p,8d,4f valence Gaussian basis set was used to describe calcium. We shall see below that these choices provide a reliable prediction of the calcium energy levels, up to the 4s5s ^{1}S levels.

An effective core potential was also used to describe the inner electrons of fluorine ([F^{7+}])[46] whereas all the electrons of C and H were considered. This actually provides an inequivalent treatment of C and F. Nevertheless, the fact of including explicitly or not the 1s electrons should be of little importance on the present results given that these electrons are anyway kept inactive in the CI treatment (see below). A (7s,7p,4d) contracted into 6s,6p,3d basis set was used for F. The 6-311++G(2d,2p) and aug-cc-pvTZ basis sets of ref 47 are used for H and C, respectively. One diffuse d and one diffuse f orbital on C were found necessary to get a reliable C−F distance when optimizing the CH_3F geometry at large Ca···CH_3F distances.

TABLE 1: Atomic Term Energies for Ca (in cm^{-1})[a]

Ca level	present calculation	experiment[52]	calculation[53]
4s4p ^{3}P	14626	15263	15121
4s3d ^{3}D	20328	20356	20620
4s3d ^{1}D	21547	21849	21965
4s4p ^{1}P	23440	23652	23434
4s5s ^{3}S	31541	31539	
4s5s ^{1}S	33281	33317	

[a] The experimental values are *j*-averaged.

3.3. Types of Calculations. Several types of calculations were completed: (a) geometry optimization for the ground state of the complex; (b) an extensive exploration of the energy variations in the ground and excited states of the complex along the Ca−*x* approach distance; (c) a limited exploration of the PES's when varying the C−F distance in CH_3F while keeping the Ca−*x* distance and the C−*x*−Ca angle fixed. More details are given now for each of these calculations.

(a) The geometry optimization is performed at the CCSD(T) level for the ground state of the system. It includes the Ca−*x* distance, the C−*x*−Ca bending angle, the C−H and C−F distances and the umbrella angle of CH_3. However, it considers CH_3F as a regular tetrahedron, with two H-atoms off the C−*x*−Ca plane by +60° and −60° and the third one in the C−*x*−Ca plane. The C−*x*−Ca angle is defined as shown in Figure 1, with respect to the H-atoms. The optimization completed included a correction for the basis set superposition error as explained in section 5.1.

(b) The energy variations for the excited states of the complex were explored as a function of the approach distance Ca−*x*, the C−*x*−Ca bending angle being set to 170°. The other coordinates defining the geometry of the system where excited states are to be calculated (i.e., the C−H and C−F distances and the umbrella angle of CH_3) are optimized for the ground state at each Ca−*x* distance with the C−*x*−Ca angle set to 170°, because above the ground state calculation is performed at the CCSD(T) level. In addition to providing geometries for the excited state calculation, this also provides the variation of the CCSD(T) potential energy along the Ca−*x* coordinate. A state-averaged MCSCF calculation, followed by RSPT2 (precisely the RS2C option of the MOLPRO package[48,49]), was performed. The average includes the 10 lowest singlet states that correlate adiabatically to the 4s^2 ^{1}S, 4s4p ^{1}P, 4s3d ^{1}D, and 4s5s ^{1}S levels of calcium at large Ca−CH_3F distances. [Only singlet states are relevant for the comparison with the experimental action spectra because transitions to the triplet states from the singlet ground state are forbidden.] The active space consists of two electrons in 13 orbitals (asymptotically the orbitals 4s, 4p, 3d, 5s and 5p of Ca). The relevance of the RSPT2 calculation to describe the atomic excited states can be seen in Table 1 where the asymptotic energies at large separation between Ca and CH_3F are compared with the experimental excited energies of free Ca. Because the orbitals are obtained from a state-averaged MCSCF calculation, we do not expect that the weakly bound ground state of the complex, even at the RSPT2 level to be accurate as the CCSD(T) calculations mentioned above which have been used to provide information on the ground state.

(c) The exploration of the PES's along the C−F coordinates was limited to the vicinity of their minima in the entrance

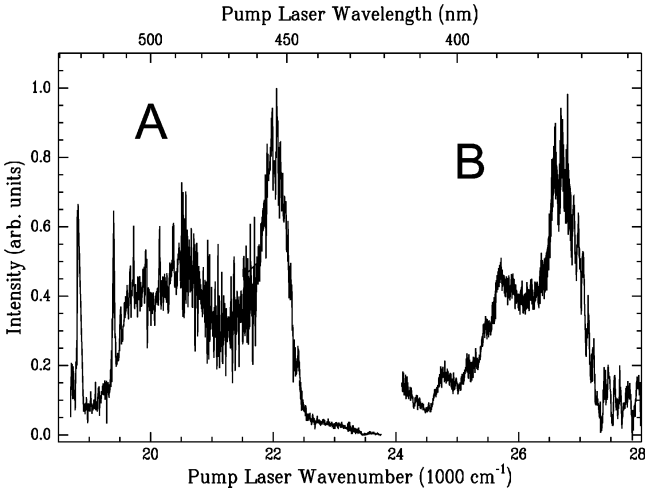

Figure 2. Action spectrum for producing electronically excited CaF in a 1:1 Ca···CH_3F complex.

channel, the main goal being to be able to estimate vibrational properties along the C−F coordinate.

4. Experimental Results

The action spectrum observed in the present experiment while monitoring CaF is shown in Figure 2. It reveals two bands labeled A and B in the figure. Only the spectral region corresponding to band B could be documented in our former CICR experiment due to the limited range achievable using a *cw* laser to excite the complex.[1] With the purpose of the present paper, the discussion below concentrates on the comparison between band B of the present action spectrum (free complex) and the band measured in the CICR experiment. Figure 3 presents this comparison. A full discussion of the A and B bands of the free complex action spectrum in Figure 2 is beyond the scope of the present paper. It will appear in paper 3 of this series.

The similarity between band B and the CICR spectrum presented in Figure 3 is striking, but qualitative. The main features of the CICR spectrum serve as a guideline to examine the similarities and differences between the two spectra. First, the CICR spectrum is structured with three features at 24 960, 25 910, and 26 780 cm^{-1}, respectively. These resolved bands appear blue shifted by 200 cm^{-1} with respect to corresponding features of the free complex spectrum as indicated by the dashed vertical lines in Figure 3. Additional structures exist in the CICR spectrum, one of which appears as an intense broad shoulder in the blue wing of the central peak near 26 100 cm^{-1}. For reasons that will be given in the Discussion, we tentatively assign this shoulder in the CICR spectrum to be a red shifted reminiscence of the very structured blue wing of the free complex spectrum. This correspondence is indicated in the figure by dot-dashed Gaussian shaped peaks. The peaks were drawn with the same width, 460 cm^{-1}, in both experiments but the CICR peak was red shifted by 650 cm^{-1} with respect to the corresponding peak in the free complex experiment. Note the width chosen is somewhat arbitrary as it is dependent on the intensity of the peak. However, the important point is that the corresponding peak is red shifted when when the complex is solvated on argon whereas the other features are blue shifted.

5. Calculation Results

5.1. Optimum Geometry in the Ground State. As already mentioned, the optimization is performed at the CCSD(T) level.

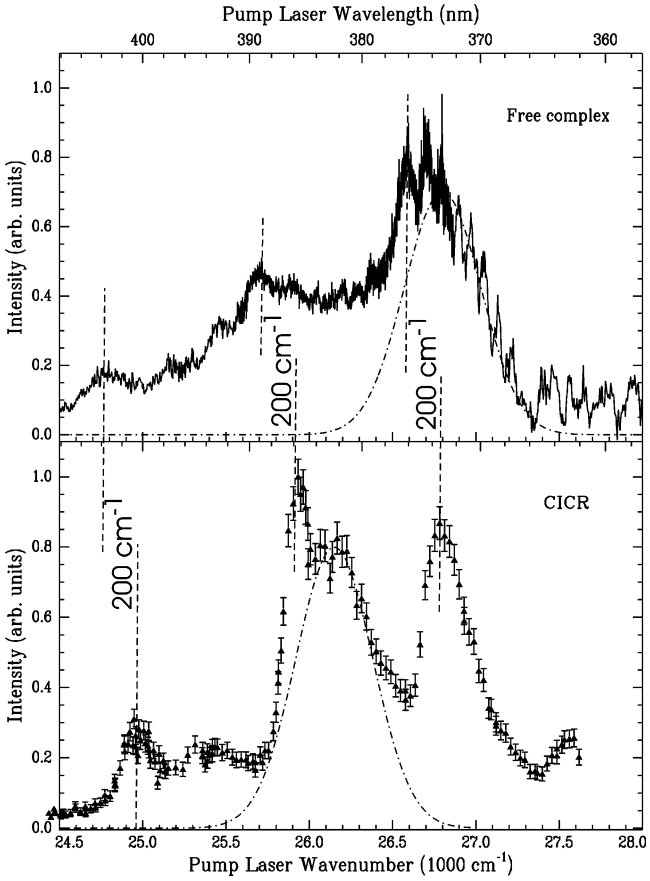

Figure 3. Band B of the action spectrum shown in Figure 2 (top panel). The bottom panel recalls the action spectrum measured in a previous CICR experiment where the Ca···CH_3F complex is deposited at the surface of a large argon cluster and CaF(A,B) monitored by its fluorescence.[1] The dotted dashed Gaussian curves are plotted to help the discussion.

It is corrected as it will appear below for the basis set superposition error (BSSE correction). The optimum geometry corresponds to the Ca atom located near the F atom of the CH_3F molecule in a bent Ca−F−C geometry. It is defined by the distances Ca−x = 2.67 Å, C−F = 1.43 Å and C−H = 1.09 Å, and by the values 220° and 107° for the bending angle C−x−Ca and the pyramidalization angle of the CH_3 group, respectively. This optimum geometry is stabilized by 850 cm^{-1} with respect to the Ca + CH_3F asymptote. [In preliminary calculations, we have identified a much deeper well on the ground state PES, which corresponds to an inserted structure $FCaCH_3$ connected without any barrier to the CaF + CH_3 asymptote. We can provide an estimate of the dissociation energy, 2.4 eV with respect to CaF + CH_3, i.e., 3.2 eV below the Ca + CH_3F asymptote. It is separated from the present well by a very high barrier that cannot be overcome under the present experimental conditions. Such a deep insertion well has been identified in a CCSD(T) type investigation of the entire ground state PES of a similar system, Ca/HF.[38]]

Of course when the CH_3 group is allowed to rotate freely about the C−F axis, there is an almost isoergic path corresponding to a circular groove about the axis. In the planar cut to the ground state PES that is defined in Figure 1, the groove appears simply as two quasi degenerate minima at C−x−Ca angles of 140 and 220°. They appear in Figure 4, a cut of the ground state PES along the bending angle C−x−Ca when Ca moves in the plane defined in Figure 1. The squares (fitted by the dashed curve) in the figure were provided by a CCSD(T) calculation where all the coordinate but the C−x−Ca angle were

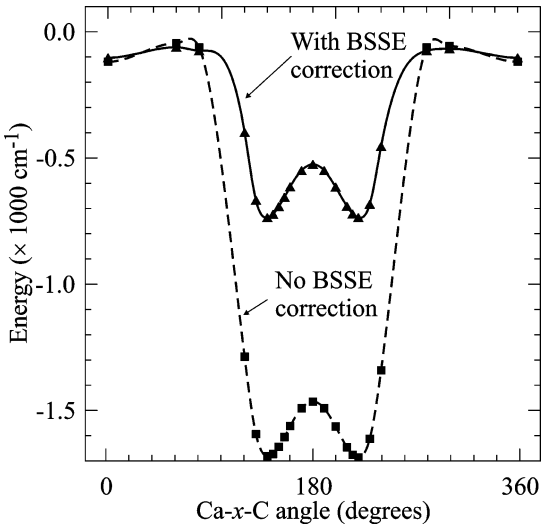

Figure 4. Calculation of the Ca···CH_3F ground state at the CCSD(T) level with the geometry optimization described in the text. The ground state energy (full triangles and solid line) is shown as a function of the bending angle C−*x*−Ca after correction for the BSSE (see the text). The dashed curve (and squares) shows the BSSE uncorrected curve. The origin of the energies corresponds to the dissociation of the complex as Ca($4s^2$ $^1S_0$) + CH_3F.

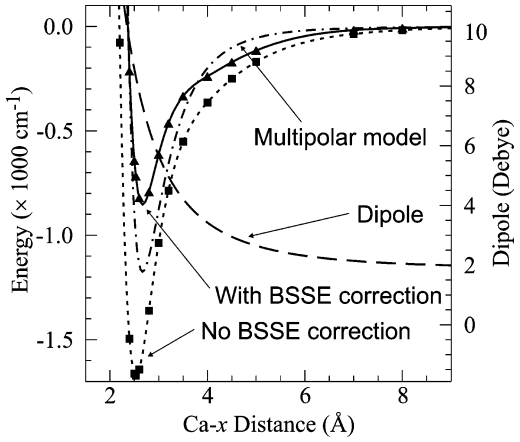

Figure 5. Same as Figure 4 but the ground state energy is shown as a function of the Ca−*x* distance. The full curve and triangles correspond to BSSE corrected potential energies, whereas the dashed curve and squares show uncorrescted energies. The dotted-dashed and dashed lines refer respectively to the energy and dipole calculations in the multipolar interaction model discussed in section 6.

adjusted to minimize the potential energy. Then a BSSE correction is performed using the counterpoise method of Boys and Bernardi for the fragments Ca and CH_3F.[50] As observed in the figure, the BSSE correction reduces the depth of the two minima by more than a factor of 2 (745 versus 1677 cm^{-1}) but does not affect their location. The region of the wells, between 120 and 240°, is indeed the region where the complex is the most compact, hence maximizing the effect of the ghost orbitals. [The value of 745 cm^{-1} is smaller than the stabilization energy of the optimum geometry, 850 cm^{-1}, because the BSSE correction changes slightly the Ca−*x* equilibrium from 2.52 Å where the present calculation is performed to 2.67 Å at the equilibrium geometry.]

The two minima that appear in the figure are part of a broad well of ≈745 cm^{-1}. Comparatively, the 220 cm^{-1} barrier between the two minima is significant.

Figure 5 reports ground state potential energy as a function of the approach distance Ca−*x*. The bending angle C−*x*−Ca is set to 220° in this calculation, which is the CCSD(T) calculation described in section 3.3b. Again, two results are shown in the figure, whether the BSSE correction is included (solid line and triangles) or not (dashed line and squares). A well depth of 850 cm^{-1} is found along the BSSE corrected curve, corresponding to the equilibrium geometry of the Ca···CH_3F complex. The BSSE correction reduces the well depth by a factor 2 (850 versus 1677 cm^{-1}) but as mentioned above it also affects the equilibrium distance (Ca−*x* = 2.67 Å along the BSSE corrected curve, versus 2.52 Å without BSSE).

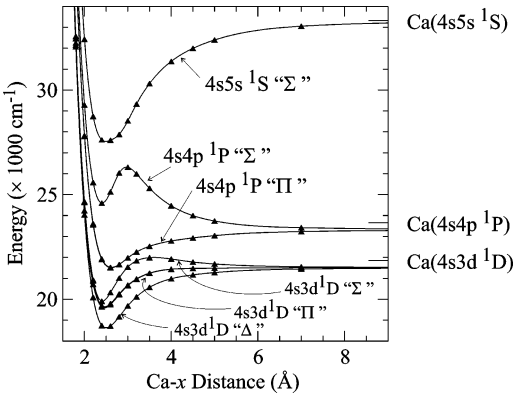

Figure 6. Same as Figure 5 for the excited singlet state calculation at the RSPT2 level as a function of the Ca−*x* distance. The labels giving asymptotic energy levels are placed at their experimental values.

5.2. Excited Potentials along the Ca−x Distance. The excited potentials shown in Figure 6 correlate to the 4s3d ^1D, 4s4p ^1P and 4s5s ^1S of Ca. They are labeled with their asymptotic correlation as in $C_{\infty v}$ because the symmetry lowering due to the nonlinearity of the Ca−F−C assembly and that due to the presence of the H atoms is weak. Nevertheless, the state labeling is put between quotation marks to stress the approximate character of the symmetry. The curves labeled "Π" and "Δ" appear doubly degenerated on the scale of the figure whereas they are not rigorously identical in the calculation. The three "Σ" curves exhibit severe anti-crossings. In contrast, the two "Π" are almost parallel.

The overall shape of curves correlating to 4s4p ^1P is akin to the potential curves correlating to Li($2p$ ^2P) + CH_3F that appear in ref 5, including the anti-crossing that the upper curve undergoes with a higher Σ-like curve. In the present case, the 4s4p ^1P "Π" curve is stabilized by 2000 cm^{-1} with respect to the 4s4p ^1P asymptote. The well depths of the curves that correlate adiabatically with the 4s3d ^1D asymptote are 1530, 1940 and 2910 cm^{-1}, respectively.

To help the discussion on the nature (valence, Rydberg or charge transfer) of the electronic excited states in the Ca···CH_3F complex, permanent dipole moments were also calculated at the RSPT2 level as a function of the Ca−*x* distance. Those associated with the molecular states $4s^2$ ^1S "Σ", 4s4p ^1P "Π", 4s4p ^1P "Σ" and 4s5s ^1S "Σ" are shown in Figure 7. The left panel of the figure shows the projection of these dipole moments along the C−F axis. The positive direction is from F to C; hence the positive dipole values at large Ca−*x* distance correspond to $F^{\delta-}C^{\delta+}$. The right panel shows the module of these dipoles. Interestingly, the left panel of the figure shows that the projection of the permanent dipole associated with the 4s4p ^1P "Σ" molecular state changes sign and becomes negative at short Ca−*x* distances.

5.3. Potentials along the F−C Coordinate. To estimate roughly the vibrational constant for the C−F stretch in both the ground state and excited states, a limited exploration of the

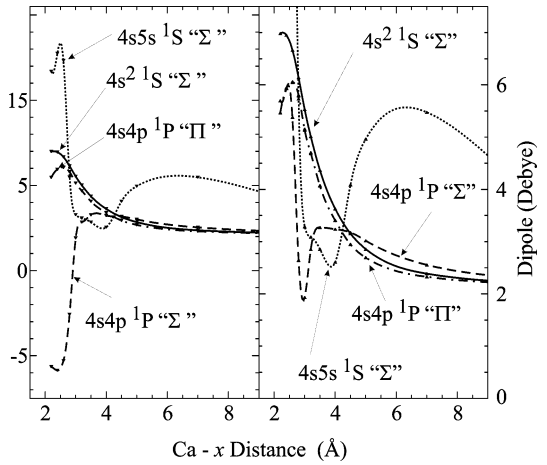

Figure 7. Permanent dipole moment of various electronic states of the Ca···CH_3F complex (as labeled in the figure) as a function of the Ca−*x* distance. The left panel shows the projection of the dipoles along the F−C axis, the positive direction being from F to C. The right panel show the module of the dipole.

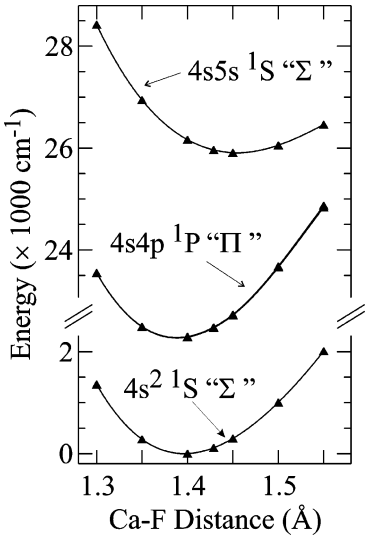

Figure 8. Potential energies at the MCSCF level as a function of the C−F distance for various electronic states of the Ca···CH_3F complex (as labeled in the figure).

PES's was performed as a function of the C−F distance. Figure 8 shows the results for states that are relevant for the discussion, i.e., the ground state and the states correlating adiabatically to Ca(4s4p $^1P_1$). Only the F and CH_3 moieties are considered to calculate the reduced mass of the oscillator and get vibrational constants from these curves. This is very approximate, but sufficient for the present purpose given that the C−F bond is much stronger than the Ca−CH_3F one. The resulting ω_e value is 960 cm^{-1} for the ground state, and 1065 and 770 cm^{-1} respectively for the 4s4p $^1P_1$ "Π" and 4s4p $^1P_1$ "Σ" curves.

6. Discussion

6.1. Electronic Structure and Geometry of the Ground State Complex. The ground state PES cut along Ca−*x* and BSSE corrected is shown in Figure 5 (solid curve and triangles). As already stated, the well of 850 cm^{-1} that appears at a 2.67 Å Ca−*x* distance corresponds to a relative minimum of the ground state PES in the entrance channel of the reaction. The actual well depth is probably larger than 850 cm^{-1} because the counterpoise BSSE correction may be overestimated. Such a deep well depth is consistent with the experimental observation that Ca···CH_3F complexes are easier to form than Ca···Ar van der Waals complexes. Finally, the calculated well depth is also consistent with observations that will be reported in Paper 3 of this series where the well depth is bracketed in the range 900−1600 cm^{-1} from threshold considerations on the complex dissociation.

The equilibrium geometry of the ground state complex at the bottom of the 850 cm^{-1} well corresponds to a C−F bond length of 1.43 Å. This value is longer than the 1.39 Å value calculated for the free CH_3F molecule. Notice that the latter value for CH_3F is quite close to the experimental value of 1.382 Å[51] and to that of a comparable calculation (1.395 Å[23]). The lengthening of the C−F bond in the complex may be considered as due to some charge transfer from Ca to CH_3F, enhancing the negative charge carried by F. However, if not fully excluded, this effect is very small. A simple dipole−induced dipole approximation of the Ca···CH_3F interaction was made indeed, assuming a 1.85 D permanent dipole in CH_3F as in the free molecule and a 25 Å^3 polarizability on Ca as in the free atom.[51] This interaction was used to provide the attractive part of a 6-12 Lennard-Jones potential, the repulsive part being adjusted to reproduce the 2.67 Å equilibrium distance of the complex. As observed in Figure 5, the resulting potential curve (dot dashed curve) is between the BSSE corrected and uncorrected CCSD(T) calculation. Moreover, the same dipole−induced dipole model was used to estimate the dipole of the complex. It is shown as a dashed curve in Figure 5 and compares well with the ab initio dipole shown in Figure 7.

When the free complex experiment is run, the Ca ···CH_3F complex is electronically excited from its ground state equilibrium geometry, a simple consequence of the Franck−Condon principle. Accordingly, in the geometry that is relevant to the free complex experiment, the Ca atom rotates almost freely in a cone of 35° around the F end of the CH_3F molecule. When turning to the CICR experiment where the complex is deposited on an argon cluster, we do not expect that the complex geometry is changed dramatically, except for the C−*x*−Ca bending angle that is probably fairly blocked inside this cone by the argon environment. This can be anticipated because the Ca−Ar (87 cm^{-1} [44]) and of CH_3F−Ar (estimated to 200 cm^{-1}) interaction energies are fairly small compared with the Ca-CH_3F binding energy (850 cm^{-1}). This expectation is consistent moreover with the qualitative similarity between the two action spectra shown Figure 3.

6.2. Assignation of Bands A and B in the Action Spectrum. The first step in the interpretation is to assign bands A and B of the present action spectrum to specific molecular states of the complex. For this purpose, the action spectrum of Figure 2 is drawn in Figure 9 together with the potential curves of Figures 5 and 6. Doing so, the action spectrum was shifted by 850 cm^{-1} with respect to that of Figure 2 to account for the energy origin that was chosen to draw the theoretical curves. Of course, this does not take into account the zero point energy in the ground state. This is reasonable, however, because the zero point energy is due mostly to the CH_3 group and is unchanged by the electronic excitation.

Band A of the action spectrum is considered first. With the energy origin of Figure 9, it covers the range 18 400−21 600 cm^{-1}. The Franck−Condon region corresponding to the Ca−*x* distance of 2.67 Å is shown as a vertical line. It crosses the excited potential curves of this energy region at 18 830, 19 930 and 20 484 cm^{-1}. According to the Franck−Condon picture, these values should correspond to maxima in the absorption of the complex. If no dynamical effect forces an additional internal

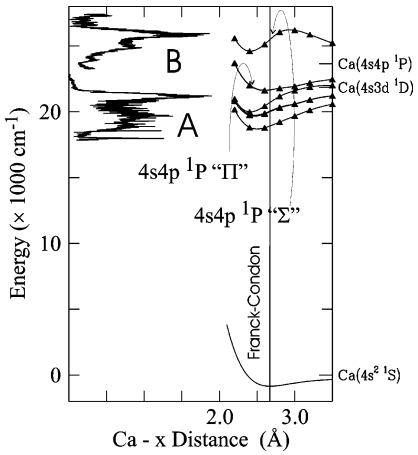

Figure 9. Compilation of the experimental results of Figures 2 with the theoretical potentials of Figures 5 (BSSE corrected) and 6. The energy origin is that of Figures 5 and 6 and the experimental spectrum is shifted accordingly (see text).

excitation of the complex to turn on the reaction, these values should correspond also to maxima in the action spectrum and the two extreme values should determine the range where band A is expected. In fact, the predicted band is located within band A of the action spectrum and is narrower by almost a factor of 2 than that observed experimentally. A part of the discrepancy is probably related to inaccuracies in the calculations that could be on the order of 200−400 cm^{-1}. Because experimental uncertainties are also possible, as mentioned in section 2 regarding the detailed structure of band A, the dynamics of the reaction associated with the excitation to this band is not discussed further.

Band B of the action spectrum is examined now. It is structured and covers the range 23 800−26 800 cm^{-1} with the energy origin of Figure 9. It overlaps a region crossed by the potential curves 4s4p ^{1}P "Σ" and 4s4p ^{1}P "Π". Very simply, we assign band B of the action spectrum to transitions toward these molecular states. As already noted in the Calculation Results, these two potential branches show an analogy with those responsible for the LiF action spectrum in the Li···CH_3F work of Polanyi and co-workers (compare Figure 7 of ref 5 to the present Figure 9). However, the detailed comparison between the two action spectra and more specifically the relative location of their most intense features with respect to the relevant potential branches suggests very substantial differences in the dynamics of the two reactions. Hence the question in the present Ca···CH_3F study, is to relate electronic excitations and reactional processes.

6.3. Reaction Mechanisms after Excitation toward Band B. *6.3.1. Partial Charge Transfer Mechanism.* The excitation of the complex in band B corresponds to the Franck−Condon region toward the curves that correlate to Ca(4s4p ^{1}P). It is indicated on the vertical line in Figure 9. This suggests two absorption maxima, one at 21 520 cm^{-1} for the intercept with the almost degenerated Π-like curves and the other at 25 500 cm^{-1} for the intercept with the Σ-like curve.

The bluer of these maxima, at 25 500 cm^{-1}, falls close to the maximum that marks the blue edge of band B in the action spectrum (25 700 cm^{-1}). This suggests that the blue part of band B is due to the excitation of the complex toward the " Σ" molecular state correlating *adiabatically* to Ca(4s4p ^{1}P). To unravel the corresponding reaction mechanism, we need to examine the electronic configuration of this state and its properties in terms of electron localization and dipole moment.

The region of interest along the 4s4p^{1}P, Σ curve is the suspended well at $R_e \approx 2.3$ Å, the origin of which is better viewed in Figure 6. It is due to an anti-crossing between this curve and the upper 4s5s^{1}S "Σ" curve. The two curves exchange their electronic character at the anti-crossing that is located when Ca−$x \approx 3$ Å. Hence, the reaction is due to an excitation that promotes the complex toward a state correlating *adiabatically* to Ca(4s4p ^{1}P) and *diabatically* to Ca(4s5s ^{1}S). The diabatic correlation indicates a large stabilization, likely related to a substantial electron transfer from excited Ca to CH_3F. This is substantiated below from general considerations on the permanent electric dipoles shown in Figure 7.

We recall that the value of +2.1 D calculated at large Ca−x separation corresponds to a permanent dipole with CH_3F polarized as $F^{-\delta}C^{+\delta}H_3$. Two situations can occur when approaching calcium. The first one presumes no electron transfer from Ca to FCH_3 and at long distances calcium is simply polarized by the electric field due to the permanent dipole of FCH_3. Hence, an additional dipole is centered on calcium, providing the following charge distribution $^{-\delta'}Ca^{+\delta'}\cdots F^{\delta-}C^{\delta+}H_3$ and the dipole moment of the complex increases as the Ca−x separation is decreased. Of course, the importance of the effect depends on the polarizability of the state of calcium under consideration, which is obviously larger for Rydberg states. However, at a short distance, in this latter case, the situation is complicated by the fact that one tends toward a complex with an inner $CaCH_3F^+$ core surrounded by the diffuse electron. The dipole is then essentially determined by the shape of the excited electron orbital. The second situation is expected in the case of electronic excitation whenever the upper state becomes a charge transfer state. In this case, the electron distribution may become $Ca^+F^-CH_3$ and the dipole moment negative.

Both situations can be observed in Figure 7. Not surprisingly, the transferless one is encountered when calcium is in the ground state (curve labeled 4s^2 ^{1}S "Σ"). The dipole moment of state 4s4p ^{1}P "Π" also appears as transferless. Starting from separation, the dipole increases slowly and smoothly for the two states indicating that their electron configuration does not change significantly when Ca approaches CH_3F. In contrast, the dipole moments of states 4s4p ^{1}P "Σ" and 4s5s ^{1}S "Σ" do not have a regular behavior. We start with the upper state 4s5s ^{1}S "Σ". At large Ca−x distances the corresponding dipole is positive, +5 D and more, consistent with the Rydberg character and large polarizability associated with Ca(4s5s ^{1}S). When Ca−$x \leq 6$ Å, the dipole along 4s5s ^{1}S "Σ" loses the asymptotic character and begins to decrease. This is due to an adiabatic mixing with a charge transfer configuration which becomes dominant at shorter distance. In addition, a further change occurs around 3 Å, the present state undergoes an anti-crossing with state 4s4p ^{1}P "Σ". Hence, the decrease of the dipole moment must be followed (diabatically) on the inner part of latter curve. The dipole goes down to less than −5 D, indicating a substantial charge transfer character to this state where the system resemble $Ca^+F^-CH_3$. We now discuss the "Σ" state dissociating into 4s4p ^{1}P. From the long distance range its dipole moment remains moderately positive, increasing from +2.1 to +3 D. Below the anticrossing region, one may consider that the diabatic extension of the state is actually the inner part of the 4s5s ^{1}S "Σ" state. The dipole goes up to +17 D and corresponds to a distorted diffuse 5s electron in the field of the Ca^+CH_3F core.

Returning to the reaction mechanism corresponding to excitation toward the suspended well on the adiabatic 4s4p ^{1}P "Σ" molecular state. From the above discussion, we know that this molecular state has a significant charge transfer character

in the excitation region. Hence, we infer that the corresponding reaction mechanism implies an electron transfer as the initial step. Because the maximum of the action spectrum and that predicted for excitation of the charge transfer state are close together, we anticipate that no additional barrier or only a quite weak one has to be overcome when the reaction is initiated by this excitation. However, this does not mean that a direct pathway exists to the reaction. The amount of electron transfer in the excited state may indeed not be sufficient for the system to evolve along a repulsive CH_3-F^- coordinate as in a standard harpoon picture. Instead, Figure 8 suggests that the excited system is formed close to a well along the C−F coordinate, implying that a barrier prevents the reaction in this PES. Hence, the barrierless character of the reaction suggests that it proceeds as explained in ref 23 for the excited $Ba\cdots CH_3F$ reaction, by an internal conversion to a lower electronic state. This mechanism is named the *partial charge transfer mechanism* hereafter to make the point that it does not reduce to a simple harpoon picture. A full analysis of this mechanism cannot be done without the simultaneous analysis of the dissociation of the complex as $Ca + CH_3F$. The two processes, reaction and dissociation, are indeed competing. Such an analysis is beyond the scope of the present paper and will appear in paper 3 of this series. The point here is simply the charge transfer character of the excitation.

The *partial charge transfer mechanism* is actually one of those proposed in ref 1 to account for the action spectrum in the CICR experiment. With the present discussion it accounts for the blue part of band B in the action spectrum of the free complex and has yet to be disentangled from other contributions. This is performed now as announced in the Introduction. Because the excited molecular state involved by this mechanism has a charge transfer character that does not exist in the ground state complex, the corresponding feature in the CICR action spectrum is expected to be red shifted with respect to the corresponding one in the free complex experiment. The analysis suggested by the dot−dashed Gaussian peak in Figure 3 supports this idea: the Gaussian peak defines the blue side of band B in the free complex experiment and with the same width and a red shift of 650 cm^{-1}, it matches the shoulder that appears in the central peak of the CICR spectrum.

6.3.2. C−F Stretch Reaction Mechanism. At this point, the *partial charge transfer mechanism* accounts for the blue side of band B in the action spectrum of the free cluster experiment and for a shoulder in the central peak of the CICR experiment. The rest of the two action spectra is thus related to another mechanism, the signature of which is the series of three peaks that appear both in the free complex and in the CICR spectra. They are marked by dashed lines in Figure 3, at 24 760, 25 710 and 26 580 cm^{-1} in the free complex spectrum and blue shifted by 200 cm^{-1} in the CICR spectrum. The almost equal spacing between the dashed lines suggests a vibrational progression. It was assigned tentatively in ref 1 to the C−F stretch.

Inspection of Figure 9 reveals a series of three peaks at 23 910, 24 860 and 25 730 cm^{-1}, respectively. The first band appears between the Π-like and the Σ-like potential curves correlating adiabatically to Ca(4s4p ^{1}P). Hence, extending the suggestion made in ref 1, we assign this series of peaks to the C−F vibrational progression originating in the well of the "Π" curve. The latter was calculated to be located at 21 515 cm^{-1} and the C−F vibrational frequency to be 1065 cm^{-1}. In that case, the series of peaks would correspond to the excitation of the levels $v = 2-4$ of this progression. With this in mind, "experimental" values defining this well can be deduced when fitting the positions of the peaks in the figure. Values of 21 300 cm^{-1} $\omega_e = 1120$ cm^{-1} and $\omega_e x_e = 60$ cm^{-1} were found for the well depth, the vibrational constant and the anharmonicity parameter, respectively. These values are very close to the calculation, confirming the assignment.

This second reaction mechanisms goes through the direct excitation of the C−F stretch within an electronic excited state that has no electron transfer character, even less than in the ground state of the complex because the dipole moment associated with state 4s4p ^{1}S "Π" has a smaller absolute value than that associated with 4s^2 ^{1}S "Σ" (see right panel of Figure 7). This suggests that solvation by the argon environment should more effectively stabilize the ground state of the complex than the excited 4s4p ^{1}S "Π" state. Hence the action spectrum is expected to blue shift in the argon environment as observed experimentally in Figure 3.

7. Conclusion

The present paper is both experimental and theoretical. It is the second of series devoted to the photoinduced reaction forming CaF in a 1:1 $Ca\cdots CH_3F$ complex. Paper 1 of this series is a cluster isolated chemical reaction (CICR) experiment where the complex was formed at the surface of a large argon cluster and the reaction turned on by scanning a laser in the vicinity of the calcium resonance line. In the present paper, the complex 1:1 $Ca\cdots CH_3F$ complexes were formed in the pulsed supersonic expansion of a He/Ca/CH_3F mixture. They are free in the gas phase; i.e., they are not supported by a cluster. As in the CICR experiment, the reaction is turned on by a laser, but over a wide range on both sides of the calcium resonance line. This provided the action spectrum of the photoinduced reaction that gives information on the access to the transition state of the photochemical reaction. Two broad structured bands (named A and B hereafter) were found. They are extending quite far on each side of the calcium resonance line.

The experiment is complemented by CCSD(T) and RSPT2 ab initio calculations, which provided cuts through the ground and excited singlet PES's of the $Ca\cdots FCH_3$ system along a Ca−CH_3F separation coordinate. When these surfaces are explored, the ground state of the system was continuously optimized. The ground state PES also benefits of a BSSE correction with respect to the $Ca + CH_3F$ dissociation. The potential curves that are provided accordingly document directly the vertical excitation energies of the complex. A limited exploration of the PES's was performed also along the C−F coordinate, again with an optimization of the other coordinates in the ground state.

The first output of the calculation is structural information on the ground state of the $Ca\cdots CH_3F$ complex. The latter is slightly bent, with calcium close to the F end of CH_3F.

The comparison between the experimental action spectrum and the calculated molecular curves helped to assign band A of the action spectrum to the excitation of molecular states that correlate to 4s3d ^{1}D at large separation between Ca and FCH_3, whereas band B is associated with the molecular states correlating to 4s4p ^{1}P. Two reaction mechanisms could be discussed for band B. The first one involves a partial electron transfer from Ca to CH_3F. However, it cannot be reduced to a simple harpooning process because the excited complex is not expected to dissociate directly as $CaF + CH_3$. Instead, an internal conversion is likely to occur prior to reaction. In this respect, the Ca/CH_3F system is akin to the Ba/CH_3F studied in the group of Radloff and that of Ureña. No such electron transfer is implied in the second reaction mechanism that involves the deposition of two or more vibrational quanta in the C−F stretch in addition

to the electronic excitation. The electron transfer that eventually promotes the reaction likely proceeds in a later step of the reaction, through an intermediate not directly accessible by vertical excitation from the ground state of the complex.

The above analysis provides a partial understanding of the excited Ca + CH_3F reaction but further works are needed to get a full picture of the excited state dynamics of this system. We already mentioned that paper 3 of this series is going to examine the competition between the present reaction channel and the Ca + CH_3F dissociation channel of the complex. A real time experiment that probes the exit channel of the reaction, far from the Franck Condon region of the reaction is also planned to get information on the apparently late charge transfer step that promotes the reaction. Finally, thorough PE's calculations are currently underway to allow for wave packet propagation, a challenge at the moment, given the number of PES's coupled and the number of degrees of freedom expected to play a role in the dynamics.

Acknowledgment. Partial support is acknowledged from CNRS-GDR 2758, "Agrégation, Fragmentation Thermodynamique de Systèmes Complexes Isolé", from the Spanish-French bilateral grant Picasso-no 09252TM and from the European Community through the PICNIC network (Product Imaging and Correlation: Nonadiabatic Interactions in Chemistry) under contract number HPRN-CT-2002-00183.

References and Notes

(1) Gaveau, M. A.; Gloaguen, E.; Fournier, P. R.; Mestdagh, J. M. *J. Phys. Chem. A* **2005**, *109*, 9494.
(2) Karny; Zare, R. N. *J. Chem. Phys.* **1978**, *68*, 3360.
(3) Weast, R. C.; Astle, M. J.; Beyer, W. H. *Handbook of Chemistry and Physics*, 65th ed.; CRC Press: Boca Raton, FL, 1984.
(4) Piecuch, P. *J. Mol. Struct.* **1997**, *436*−*437*, 503.
(5) A. Hudson, J.; Naumkin, F. Y.; Oh, H. B.; Polanyi, J. C.; Raspopov, S. A. *Faraday Discuss.* **2001**, *118*, 191.
(6) Janssen, M. H. M.; Parker, D. H.; Stolte, S. *J. Phys. Chem.* **1991**, *95*, 8142.
(7) Wiskerke, A. E.; Stolte, S.; Loesch, H. J.; Levine, R. D. *Phys. Chem. Chem. Phys*. **1999**, *2*, 757.
(8) Husain, D.; Geng, J. F.; Castano, F.; Rayo, M. N. S. *J. Photochem. Photobiol. A*−*Chem.* **2000**, *133*, 1.
(9) Chang, X. Y.; Ehlich, R.; Hudson, A. J.; Piecuch, P.; Polanyi, J. C. *Faraday Discuss.* **1997**, *108*, 411.
(10) Chang, X. Y.; Ehlich, R.; Hudson, A. J.; Polanyi, J. C.; Wang, J. X. *J. Chem. Phys.* **1997**, *106*, 3988.
(11) Hudson, A. J.; Oh, H. B.; Polanyi, J. C.; Piecuch, P. *J. Chem. Phys.* **2000**, *113*, 9897.
(12) Liu, K.; Polanyi, J. C.; Yang, S. *J. Chem. Phys.* **1992**, *96*, 8628.
(13) Visticot, J. P.; Soep, B.; Whitham, C. J. *J. Phys. Chem.* **1988**, *92*, 4574.
(14) Soep, B.; Whitham, C. J.; Keller, A.; Visticot, J. P. *Faraday Discuss.* **1991**, *91*, 191.
(15) Krim, L.; Qiu, P.; Jouvet, C.; Lardeux-Dedonder, C.; McCaffrey, J. G.; Soep, B.; Solgadi, D.; Benoist d'Azy, O.; Ceraolo, P.; et al. *Chem. Phys. Lett.* **1992**, **200**, 267.
(16) Keller, A.; Lawruszczuk, R.; Soep, B.; Visticot, J. P. *J. Chem. Phys.* **1996**, *105*, 4556.
(17) Skowronek, S.; Pereira, R.; González Ureña, A. *J. Chem. Phys.* **1997**, *107*, 1668.
(18) Skowronek, S.; Pereira, R.; González Ureña, A. *J. Phys. Chem.* **1997**, *101*, 7468.
(19) Skowronek, S.; González Ureña, A. G. *Prog. React. Kinet. Mech.* **1999**, *24*, 101.
(20) Skowronek, S.; Jiménez, J. B.; González Ureña, A. *Chem. Phys. Lett.* **1999**, *303*, 275.
(21) Stert, V.; Farmanara, P.; Radloff, W.; Noack, F.; Skowronek, S.; Jiménez, J.; González Ureña, A. *Phys. Rev. A* **1999**, *59*, R1727.
(22) Stert, V.; Farmanara, P.; Ritze, H.-H.; Radloff, W.; Gonzalez-Ureña, A. *Chem. Phys. Lett.* **2001**, *337*, 299.
(23) Stert, V.; Ritze, H. H.; Farmanara, P.; Radloff, W. *Phys. Chem. Chem. Phys.* **2001**, *3*, 3939.
(24) Stert, V.; Ritze, H. H.; Radloff, W.; Gasmi, K.; Gonzalez-Ureña, A. *Chem. Phys. Lett.* **2002**, *355*, 449.
(25) Stert, V.; Ritze, H. H.; Radloff, W. *Chem. Phys. Lett.* **2002**, *354*, 269.
(26) Lippert, H.; Manz, J.; Oppel, M.; Paramonov, G. K.; Radloff, W.; Ritze, H. H.; Stert, V. *Phys. Chem. Chem. Phys.* **2004**, *6*, 4283.
(27) Lippert, H.; Manz, J.; Oppel, M.; Paramonov, G. K.; Radloff, W.; Ritze, H. H.; Stert, V. *Phys. Chem. Chem. Phys.* **2004**, *6*, 5086.
(28) Paniagua, M.; Aguado, A.; Lara, M.; Roncero, O. *J. Chem. Phys*. **1999**, *111*, 6712.
(29) Spirko, V.; Piecuch, P.; Bludsky, O. *J. Chem. Phys*. **2000**, *112*, 189.
(30) Mrugala, F.; Piecuch, P.; Spirko, V.; Bludsky, O. J. *Mol. Struct.* **2000**, *555*, 43.
(31) Jasper, A.; W.; Hack, M. D.; Chakraborty, A.; Truhlar, D. G.; Piecuch, P. *J. Chem. Phys.* **2001**, *115*, 7945.
(32) Jasper, A. W.; Hack, M. D.; Truhlar, D. G.; Piecuch, P. *J. Chem. Phys.* **2002**, *116*, 8353.
(33) Burcl, R.; Piecuch, P.; Spirko, V.; Bludsky, O. *J. Mol. Struct. (THEOCHEM)* **2002**, *591*, 151.
(34) Jasper, A. W.; Hack, M. D.; Chakraborty, A.; Truhlar, D. G.; Piecuch, P. *J. Chem. Phys.* **2003**, *119*, 9321.
(35) Topaler, M. S.; Truhlar, D. G.; Chang, X. Y.; Piecuch, P.; Polanyi, J. C. *J. Chem. Phys.* **1998**, *108*, 5349.
(36) Topaler, M. S.; Truhlar, D. G.; Chang, X. Y.; Piecuch, P.; Polanyi, J. C. *J. Chem. Phys.* **1998**, *108*, 5378.
(37) Isaacson, A. D.; Muckerman, J. T. *J. Chem. Phys*. **1980**, *73*, 1729.
(38) McGuire, M. J.; Piecuch, P.; Kowalski, K.; Kucharski, S. A.; Musial, M. *J. Phys. Chem. A* **2004**, *108*, 8878.
(39) De Castro, M.; Candori, R.; Pirani, F.; Aquilanti, V.; Garay, M.; González Ureña, A. *J. Chem. Phys.* **2000**, *112*, 770.
(40) Meijer, A. J. H. M.; Groenenboom, G. C.; van der Avoird, A. *J. Chem. Phys.* **1996**, *105*, 2247.
(41) Sanz, C.; van der Avoird, A.; Roncero, O. *J. Chem. Phys.* **2005**, 123.
(42) Verbockhaven, G.; Sanz, C.; Groenenboom, G. C.; Roncero, O.; van der Avoird, A. *J. Chem. Phys.* **2005**, 122.
(43) Werner, H.-J.; Knowles, P. J. MOLPRO a package of ab initio programs, version 2005, http://www.molpro.net, 2005.
(44) Spiegelman, F.; Maron, L.; Breckenridge, W. H.; Mestdagh, J. M.; Visticot, J. P. *J. Chem. Phys.* **2002**, *117*, 7534.
(45) Fuentealba, P.; Stoll, H.; Savin, A. *Phys. Rev. A Gen. Phys.* **1988**, *38*, 483.
(46) Bouteiller, Y.; Mijoule, C.; Nizam, M.; Barthelat, J. C.; Daudey, J. P.; Pelissier, M.; Silvi, B. *Mol. Phys.* **1988**, *65*, 295.
(47) Pacific Northwest National Laboratory, Gaussian Basis Set Library, http://www.cse.clrc.ac.uk/qcg/basis/, 2005.
(48) Celani, P.; Werner, H. J. *J. Chem. Phys.* **2000**, *112*, 5546.
(49) Werner, H.-J. *Mol. Phys.* **1996**, *89*, 645.
(50) Boys, S. F.; Bernardi, F. *Mol. Phys.* **1970**, *19*, 553.
(51) Lide. D. R., Ed. *Handbook of Chemistry and Physics*, 77th ed.; CRC Press: Boca Raton, FL, 1996.
(52) Sugar, J.; Corliss, C. *J. Phys. Chem. Ref. Data* **1979**, *8*, 865.
(53) Czuchaj, E.; Krosnicki, M.; Stoll, H. *Chem. Phys.* **2003**, *292*, 101.